Stopbands for lower-order Lamb waves in one-dimensional composite thin plates

Jiu-Jiu Chen, Kai-Wen Zhang, Jian Gao, and Jian-Chun Cheng*
Laboratory of Modern Acoustics and Institute of Acoustics, Nanjing University, Nanjing 210093, China
(Received 8 October 2005; revised manuscript received 24 February 2006; published 31 March 2006)

We study theoretically the propagation of lower-order Lamb waves in one-dimensional composite thin plates. The dispersion curves of Lamb modes propagating parallel to the surfaces of the thin plates in the periodic direction are calculated based on the plane wave expansion method. The existence of band gaps for low-order Lamb wave modes is demonstrated in the systems made of alternating strips of tungsten materials and silicon resin. The finite element method is employed to calculate the transmitted power spectra, which is in good agreement with the results by plane wave exposition. A crucial parameter, i.e., the ratio of the plate thickness (L) to the lattice spacing (D), is discussed in detail for the influence of formation of band gaps.

DOI: 10.1103/PhysRevB.73.094307 PACS number(s): 63.20.−e, 62.65.+k, 41.20.Jb, 43.20.+g

I. INTRODUCTION

In the last few years, the existence of forbidden gaps in the band structure of acoustic (AC) and elastic (EL) waves propagating in periodic composite materials has received a great deal of attention.[1–7] For frequencies within the band gap, the propagation of acoustic or elastic waves is forbidden in all directions, thus suggesting various applications such as acoustic filters, ultrasonic silent blocks, acoustic mirrors, etc. Up to now, bulk and surface acoustic waves in elastic periodic structures have been studied both theoretically[8–20] and experimentally.[21–26]

On the other hand, there has been a growing interest in using Lamb waves for a variety of physical, chemical, and biological sensors. The Lamb waves also have potential application to noncontact and nondestructive evaluation and characterization of sheet materials in industry.[27] The operating principle of Lamb wave sensors is similar to the more extensively studied surface acoustic wave (SAW) sensors.[28] Important advantages over the SAW sensors are obtained by utilizing the low-order antisymmetric Lamb wave mode, the A_0 mode, which propagates in thin plate that is only a few micrometers thick. It is certainly more complicated to study the elastic waves in the composite plate than that of bulk and surface acoustic waves due to longitudinal and transversal strain components which couple to each other by reflections at the plate boundaries with complex wave vectors (Lamb waves).

The first attempt to describe the propagation of Lamb waves with wavelength comparable with the lattice is due to Auld and co-workers,[29,30] who studied two-dimensional composites within the couple-mode approximation. Alippi *et al.*[31] have presented an experimental study on stopband phenomenon of lowest-order Lamb waves in piezoelectric periodical composite plates and interpreted their results in terms of a theoretical model, which provides approximate dispersion curves of the lowest Lamb waves in the frequency range below the first thickness mode by assuming no coupling between different Lamb modes. The transmissivity of the finite structure to Lamb wave modes was also calculated by taking into account the effective plate velocities of the two constituent materials.[32]

However, up to now, to our knowledge, there is still no study on propagation of the Lamb wave in periodical composite plate based on a rigorous theory of elastic wave. Therefore, it is significant to study propagation of Lamb waves in the periodic composite systems. In this paper, we present a theoretical calculation for the dispersion curves of lower-order Lamb waves in one-dimensional (1-D) composite thin plates based on a rigorous theory by the plane wave expansion (PWE) method. The existence of band gaps for low-order Lamb wave modes in the composite thin plates is demonstrated for some ranges of the ratio of the plate thickness to lattice spacing. The stopbands calculated for 1-D periodic structure by PWE method are in good agreement with the results obtained by the finite element (FE) method. A crucial parameter, i.e., the ratio of the plate thickness (L) to the lattice spacing (D), is discussed in detail for the influence of formation of band gaps in the dispersion curves.

The paper is organized as follows: In Sec. II we derive the general equation of motion for the 1-D composite thin plate that supports Lamb wave modes. In Sec. III, numerical results calculated for 1-D periodic structure by PWE are given and the existence of band gaps for lower-order Lamb wave modes is demonstrated for some ranges of L/D. In Sec. IV, the FE method is employed to calculate the transmitted power spectra (TPS), which is in good agreement with the results from PWE. The final section contains the concluding remarks.

II. FORMULATIONS

As shown in Fig. 1, we suppose that the periodic composite plate consists of material A with width d_A, material B with width d_B, lattice spacing $D=d_A+d_B$, and filling rate f defined by $f=d_A/D$. The wave propagates along the x direction of a

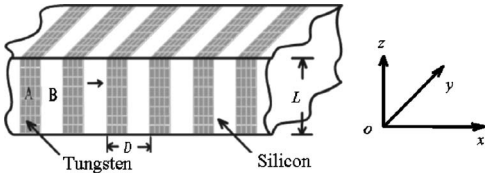

FIG. 1. The 1-D periodic composite plate consisting of alternate tungsten and silicon strips.

 ©2006 The American Physical Society

plate bounded by planes $z=0$ and $z=L$. We consider a two-dimensional problem, in which all field components are assumed to be independent of the y direction.

In an inhomogeneous linear elastic medium with no body force, the equation of motion for displacement vector $\boldsymbol{u}(x,z,t)$ can be written as

$$\rho(x)\ddot{\boldsymbol{u}}_p = \partial_q[c_{pqmn}(x)\partial_n \boldsymbol{u}_m], \quad p=1,2,3, \tag{1}$$

where $\rho(x)$ and $c_{pqmn}(x)$ are the x-dependent mass density and elastic stiffness tensor, respectively. Due to the spatial periodicity in the x direction, the material constants, $\rho(x)$ and $c_{pqmn}(x)$, can be expanded in the Fourier series with respect to the 1-D reciprocal lattice vectors (RLVs). From the Bloch theorem and by expanding the displacement vector $\boldsymbol{u}(x,z,t)$ into Fourier series, one obtains

$$\boldsymbol{u}(x,z,t) = \sum_G e^{jk_x x - j\omega t}(e^{jGx}\boldsymbol{A}_G e^{jk_z z}), \tag{2}$$

where k_x is a Bloch wave vector, ω is the circular frequency, $\boldsymbol{A}_G=(A_G^1,A_G^2,A_G^3)$ the amplitude is the amplitude vector of the partial waves, and k_z is the wave number of the partial waves along the z direction. Substituting Eq. (2) into Eq. (1), one obtains homogenous linear equations to determine both (A_G^1,A_G^2,A_G^3) and k_z. Supposing that the materials A and B are cubic materials, it is obvious that the wave motion polarized in the y direction, namely *SH* wave, decouples to the wave motions polarized in the x and z directions, namely, *P* and *SV* waves. We focus our attentions on *P* and *SV* waves because it is relatively simple to discuss the *SH* wave. If one truncates the expansions of Eq. (2) by choosing n RLVs, one will obtains $4n$ eigenvalues $k_z^{(l)}$ $(l=1-4n)$. For the Lamb waves, all of the $4n$ eigenvalues $k_z^{(l)}$ must be included. Accordingly, the displacement vector of the Lamb waves can be taken of the form

$$\begin{aligned}\boldsymbol{u}(x,z,t) &= \sum_G{}' e^{i(k_x+G)x-i\omega t}\left(\sum_{l=1}^{4n} A_G e^{iK_z^{(l)}z}\right) \\ &= \sum_G{}' e^{i(k_x+G)x-i\omega t}\left(\sum_{l=1}^{4n} X_l \varepsilon_G^{(l)} e^{ik_z^{(l)}z}\right),\end{aligned} \tag{3}$$

where $\varepsilon_G^{(l)}$ is the associated eigenvector for the eigenvalue $k_z^{(l)}$, $\mathbf{X}=[X_1,X_2,\ldots,X_{4n}]^t$ (the superscript denotes the transpose) is the weighting coefficient to be determined, and the prime of the summation expresses that the sum over G is truncated up to n.

The boundary conditions are the stress-free on the upper $(z=0)$ and rear $(z=L)$ surfaces

$$\mathbf{T}_{p3}|_{z=0,L} = c_{p3mn}\partial_n u_m|_{z=0,L} = 0 \quad (p=1,3), \tag{4}$$

where $\mathbf{T}_{pq}$ is the stress tensor and L is the plate thickness. Equation (4) will lead to $4n$ homogeneous linear equations for determining X_l $(l=1-4n)$. For the existence of a nontrivial solution of X_l, the determinant of the coefficient matrix of these equations should be equal to zero, which will bring on the dispersion relation, $\omega=\omega(k_x)$. In practice, an alternative search procedure is usually required to find these ω.[28,33]

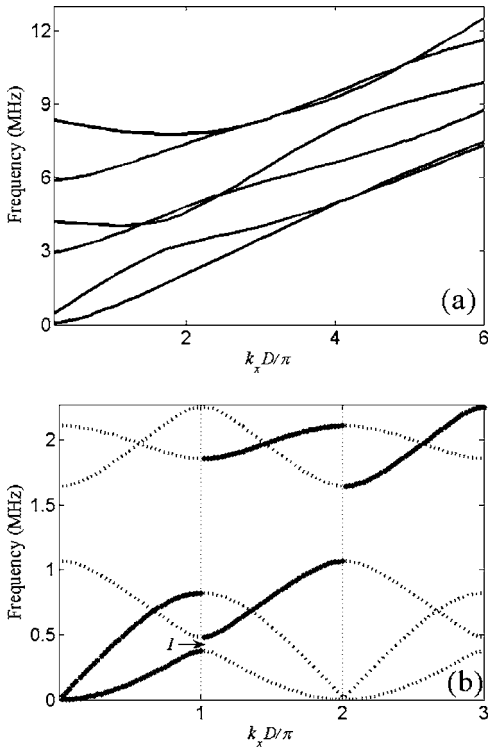

FIG. 2. Schematic representation of the dispersion curve for (a) a cubic plate (silicon) with $L=1.0$ mm and (b) the composite thin plate (tungsten/silicon) with $f=0.5$, $L=1.0$ mm, and $D=2.0$ mm.

III. NUMERICAL SIMULATIONS BY PWE METHOD

The seven RLVs are used in all numerical calculations, which results in a very good convergence for the materials (the material A and B are tungsten and silicon resin, respectively) in numerical experiments. The convergence has been checked by the fact that the dispersion curves calculated do not change at all, even if one increases the number of RLVs further. The elastic properties of the materials utilized in the numerical calculations are given in Ref. 34.

In order to demonstrate the existence of band gaps for low-order Lamb wave modes in the 1-D periodic structure, we have calculated the dispersion curve for a cubic medium (silicon) of a 1 mm thick plate by considering only the fundamental term in the Fourier and Floquet series,[33] as shown in Fig. 2(a). Figure 2(b) displays the dispersion curves of four lower-order modes along the boundary of the mini-Brillouin zone with filling ratio $f=0.5$, $L=1.0$ mm, and $D=2.0$ mm. One can obviously observe the modifications produced by resonant reflections in the strip lattice. The dashed vertical lines in Fig. 2(b) identify the wavelengths that are resonantly reflected by the periodic lattice of strips.

By comparing Fig. 2(a) with Fig. 2(b), one can easily find that there exists a band gap from 1065 to 1642 kHz for the lower-order Lamb modes propagating in the 1-D periodic structure. The gap width $(\Delta\Omega)$ is 577 kHz and the corresponding gap/midgap ratio $(\Delta\Omega/\Omega_m, \Omega_m$ is the midgap frequency) is approximately 0.426.

In order to analyze the influence of the ratio L/D for the band gap width, we also calculate the dispersion curves of

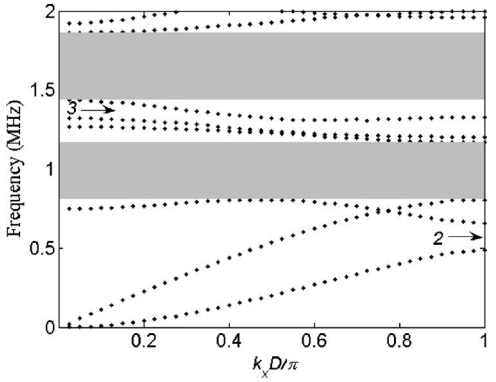

FIG. 3. Dispersion curves of Lamb wave modes for the 1-D composite plate with filling ratio $f=0.5$, $L=2.0$ mm, and $D=2.0$ mm. There are two band gaps (hatched region).

the lower-order modes with $f=0.5$, $L=2.0$ mm, and $D=2.0$ mm, as shown in Fig. 3. It is apparent that there are two band gaps (from 806 to 1167 kHz and from 1438 to 1863 kHz, respectively) for the ratio $L/D=1$. The gap widths are 361 and 425 kHz, and the corresponding gap/midgap ratios are about 0.366 and 0.255, respectively.

Basically, there are three parameters that influence the formation of band gaps, i.e., L/D, f, and the contrast between the physical parameters of the constituents. It is rather intuitive that L/D is very crucial for the formation of a band gap. Figure 4 depicts the gap width of the lowest band gap as a function of L/D with $f=0.5$ and $D=2$ mm for tungsten/silicon supperlattices. It is noteworthy to point out that the lowest band gap opens up over a domain of the ratio of L/D defined by $0.15 \leqslant L/D \leqslant 1.64$. The maximum value of gap width appears at $L/D \approx 0.53$ for the lowest band gap and reaches 610 kHz as shown in Fig. 4.

It is noted that the value of the gap width of the lowest band gap in the systems increases monotonously with the increase of the value of the ratio of L/D until a critical value and then decreases. In fact, a plate can support a number of Lamb wave modes depending on the value of the ratio L/λ, where λ is the acoustic wavelength. When the periodicity of these Lamb waves matches the lattice spacing, stopbands appear in the Lamb wave dispersion curves.[35] There is a high interaction when the wavelength of the Lamb wave is close the lattice constant, which induces mode conversion and reflections. When the wavelength of the Lamb wave is different from the periodicity of the lattice constant, the interaction is weak. On the other hand, the midgap frequency of the forbidden gap is inversely proportional to the lattice spacing D,[4] therefore, the value of the ratio of L/D is important for

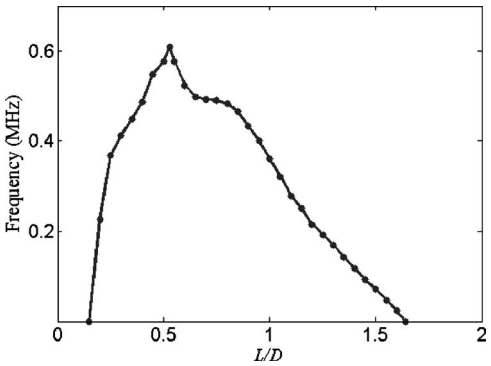

FIG. 4. The width of the lowest band gap at the filling fraction $f=0.5$ versus the value of L/D.

the width of the band gap for the Lamb waves in the periodic composite systems.

IV. TRANSMITTED POWER SPECTRUM (TPS) BY FINITE ELEMENT METHOD (FEM)

In order to demonstrate further the existence of the band gaps for the lower-order modes in the 1-D periodic structure, the FEM is employed to calculate the TPS for the finite periodic structure. The FE solution involves the discretization of the domain into a number of elements, approximating the displacement values interior to the elements in terms of its nodal value through the shape functions of the chosen element and the determination of nodal values.[21]

Figure 5 shows the configuration of the modified composite plate in the FE calculations, in which the superlattice with ten periods (the length is 20 mm) is bounded by two pure tungsten plates (the length is 100 mm) at two sides. Lamb waves are excited by the force function $f(t)$ that is a triangle wave at the $x=0$, and are received at $x=140$ mm.[36] The generation source is far from the periodic structure in order to obtain approximate plane waves when the wave fronts reach it. The step sizes of temporal and spatial discretization in the finite model are fine enough for the convergence of the numerical results (increasing the number of elements of the finite element mesh is equivalent to increasing the number of harmonic waves in PWE method). The vertical displacement of a node at the upper surface of the plate behind the superlattice array at $x=140$ mm is collected as a function of time. For a sufficiently large number of these vertical displacement data on the time axis, the displacement fields are Fourier transformed into the frequency domain to yield the TPS.

Figure 6 show the TPS for the 1-D composite structure plate with $f=0.5$, $L=1.0$ mm, and $D=2.0$ mm. There is a

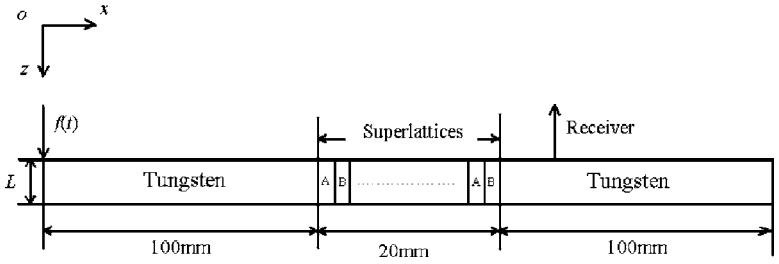

FIG. 5. Modified plate geometry in the FE calculations.

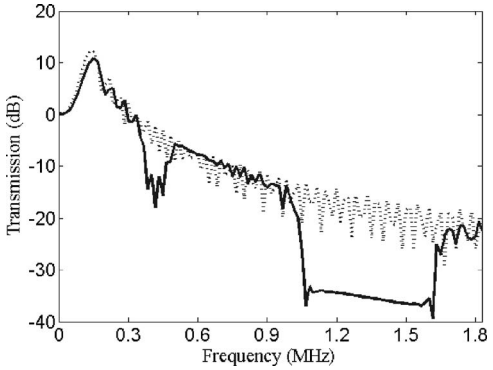

FIG. 6. The TPS computed by the FE method with $f=0.5$, $L=1.0$ mm, and $D=2.0$ mm through the composite plate (solid line) and a pure Tungsten plate (dashed line).

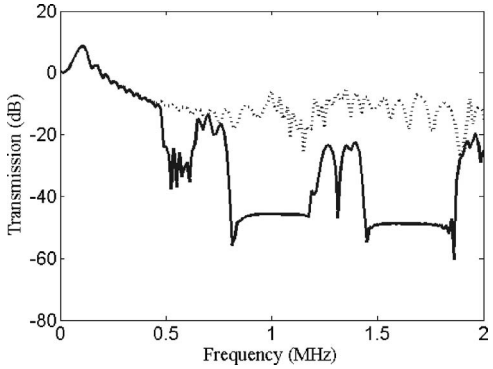

FIG. 7. The TPS computed by the FE method with $f=0.5$, $L=2.0$ mm, and $D=2.0$ mm: through the composite plate (solid line) and a pure Tungsten plate (dashed line).

broad region from 1060 to 1630 kHz that is less than −30 dB. The result shows good agreement with that by PWE method. The TPS is also depicted in Fig. 6 from a pure tungsten plate with the same dimensions, and no sharp attenuation in any frequency domain is observed, as seen in Fig. 6.

For the second sample, f, D, and the configuration are the same as the first one, and only the thickness of the plate is different ($L=2$ mm). Figure 7 depicts the TPS for the 1-D plate with periodic structure and without periodic structure. The frequency range of the gaps of Lamb waves by PWE is almost the same as those of large attenuation in the calculated TPS. The first gap extends from the frequency of 804 up to 1176 kHz and the second from 1436 to 1869 kHz, which are less than −45 dB.

It is interesting to notice that there are some slight dips centered at about 0.4 MHz in Fig. 6, or 0.5 and 1.3 MHz in Fig. 7. These dips are attributed to the band gaps of antisymmetric mode, but not the entire band gap of symmetric and antisymmetric modes, which can be observed in Figs. 2(b) and 3, indicated by the arrows 1, 2, and 3. On the other hand, the lower frequency components of the modes are mainly excited for the thin plate,[27] so that the TPS energy displays a monotonic decrease as the frequency increases as shown in Fig. 6. As the plate is thicker, the higher frequency components of the modes are also generated, so that the attenuation of the TPS energy will be slower, as shown in Fig. 7.

V. CONCLUSIONS

We have examined the band structures of lower-order Lamb wave modes propagating in the 1-D periodic composite thin plate based on the PWE for infinitely long periodic systems and have calculated the TPS for finite systems by using the FE method. As shown, the TPS through a superlattice with ten periods has prominent dips at frequencies corresponding to the gaps in band structure. A crucial parameter, namely, the ratio of L/D, was discussed, and the value of the ratio of L/D was emerging as critical parameters in determining the existence of band gaps for the Lamb waves in the periodic structures. Thus, we can achieve the needed width of band gaps for Lamb wave by varying the thickness of the plate.

ACKNOWLEDGMENTS

The work was supported by the Science Foundation of China for Excellent Youth under Grant No. 10125417, the Ministry of Education of China under Grant No. 705017, the State Key Development Program of Basic Research of China (under Grant No. 51307). We gratefully acknowledge very helpful communications with Y. Tanaka (Hokkaido University, Japan), M. Wilm (associé à l'Université de Franche-Comté, France) and Z. G. Huang (National Taiwan University). We are also thankful to T. T. Wu (National Taiwan University, China) for sending us the manuscript of Ref. 16.

*Corresponding author. Electronic address: jccheng@nju.edu.cn

[1] M. Sigalas and E. N. Economou, Solid State Commun. **86**, 141 (1993).
[2] M. S. Kushwaha and P. Halevi, Appl. Phys. Lett. **64**, 1085 (1994).
[3] M. Sigalas and E. N. Economou, J. Sound Vib. **158**, 377 (1992).
[4] M. S. Kushwaha, Appl. Phys. Lett. **70**, 3218 (1997).
[5] M. S. Kushwaha, P. Halevi, L. Dobrzynski, and B. Djafari-Rouhani, Phys. Rev. Lett. **71**, 2022 (1993).
[6] M. S. Kushwaha, P. Halevi, G. Martínez, L. Dobrzynski, and B. Djafari-Rouhani, Phys. Rev. B **49**, 2313 (1994).
[7] X. F. Wang, M. S. Kushwaha, and P. Vasilopoulos, Phys. Rev. B **65**, 035107 (2001).
[8] B. Djafari-Rouhani, L. Dobrzynski, O. Hardouin Duparc, R. E. Camley, and A. A. Maradudin, Phys. Rev. B **28**, 1711 (1983).
[9] B. Djafari-Rouhani, A. A. Maradudin, and R. F. Wallis, Phys. Rev. B **29**, 6454 (1984).
[10] S. Tamura and J. P. Wolfe, Phys. Rev. B **35**, 2528 (1987).
[11] Takashi Aono and Shin-ichiro Tamura, Phys. Rev. B **58**, 4838 (1998).
[12] Y. Tanaka and S. I. Tamura, Phys. Rev. B **58**, 7958 (1998): Physica B **263**, 77 (1999).

[13] Yukihiro Tanaka, Michiko Narita, and Shin-ichiro Tamura, J. Phys.: Condens. Matter **10**, 8787 (1998).
[14] Y. Tanaka and S. I. Tamura, Phys. Rev. B **60**, 13294 (1999).
[15] Y. Tanaka, Y. Tomoyasu, and S. I. Tamura, Phys. Rev. B **62**, 7387 (2000).
[16] Tsung-Tsong Wu, Zi-Gui Huang, and S. Lin, Phys. Rev. B **69**, 094301 (2004).
[17] Tsung-Tsong Wu, Zin-Chen Hsu, and Zi-Gui Huang, Phys. Rev. B **71**, 064303 (2005).
[18] M. Wilm, A. Khelif, S. Ballandras, V. Laude, and B. Djafari-Rouhani, Phys. Rev. E **67**, 065602(R) (2003).
[19] V. Laude, M. Wilm, S. Benchabane, and A. Khelif, Phys. Rev. E **71**, 036607 (2005).
[20] Qing Ni and Jianchun Cheng, Phys. Rev. B **72**, 014305 (2005).
[21] Shu Zhang and Jianchun Cheng, Phys. Rev. B **68**, 245101 (2003).
[22] J. O. Vasseur, P. A. Deymier, B. Chenni, B. Djafari-Rouhani, L. Dobrzynski, and D. Prevost, Phys. Rev. Lett. **86**, 3012 (2001).
[23] Y. Pennec, B. Djafari-Rouhani, J. O. Vasseur, H. Larabi, A. Khelif, A. Choujaa, S. Benchabane, and V. Laude, Appl. Phys. Lett. **87**, 261912 (2005).
[24] R. E. Vines, J. P. Wolfe, and A. V. Every, Phys. Rev. B **60**, 11871 (1999).
[25] A. G. Every, R. E. Vines, and J. P. Wolfe, Phys. Rev. B **60**, 11755 (1999).
[26] Tsung-Tsong Wu, Zi-Gui Huang, and Shih-Yang Liu, Z. Kristallogr. **220**, 841 (2005).
[27] J. C. Cheng and S. Y. Zhang, Appl. Phys. Lett. **74**, 2087 (1999).
[28] S. G. Joshi and Y. Jin, J. Appl. Phys. **69**, 8018 (1991).
[29] B. A. Auld, Y. A. Shui, and Y. Wang, J. Phys. (Paris) **45**, 159 (1984).
[30] B. A. Auld and Y. Wang, Proc.-IEEE Ultrason. Symp. 528 (1984).
[31] A. Alippi, F. Craciun, and E. Molinari, Appl. Phys. Lett. **53**, 1806 (1988).
[32] A. Alippi, F. Craciun, and E. Molinari, J. Appl. Phys. **66**, 2828 (1989).
[33] M. Wilm, S. Ballandras, V. Laude, and T. Pastureaud, J. Acoust. Soc. Am. **112**, 943 (2002).
[34] We used the elastic constants $C_A^{11}=50.2$ $C_A^{12}=19.9$ and $C_A^{44}=15.2$ (in units of 10^{11} dyn/cm^2) and mass density $\rho_A=19.2$ g/cm^3 for tungsten, and mass $C_B^{11}=16.57$ $C_B^{12}=6.39$ and $C_B^{44}=7.956$ (in units of 10^{11} dyn/cm^2) and mass density $\rho_B=2.332$ g/cm^3 for silicon.
[35] W. A. Smith and B. A. Auld, IEEE Trans. Ultrason. Ferroelectr. Freq. Control **38**, 40 (1991).
[36] Friedrich Moser, Laurence J. Jacobs, and Jianmin Qu, NDT & E Int. **32**, 225 (1999).